IEEE Access
Multidisciplinary | Rapid Review | Open Access Journal

Received April 4, 2021, accepted April 13, 2021, date of publication April 20, 2021, date of current version April 29, 2021.

Digital Object Identifier 10.1109/ACCESS.2021.3074215

Multi-Objective Comprehensive Control of Trajectory Tracking for Four-In-Wheel-Motor Drive Electric Vehicle With Differential Steering

HONGBO WANG[1,2], CHENGLEI HU[1], WEI CUI[1], AND HAIPING DU[2], (Senior Member, IEEE)
[1]School of Automotive and Transportation Engineering, Hefei University of Technology, Hefei 230009, China
[2]School of Electrical, Computer, and Telecommunications Engineering, University of Wollongong, Wollongong, NSW 2522, Australia

Corresponding author: Hongbo Wang (bob.627@163.com)

This work was supported in part by the National Natural Science Foundation of China under Grant U1564201, and in part by the Science Fund of Anhui Intelligent Vehicle Engineering Laboratory under Grant PA2018AFGS0026.

ABSTRACT For 4MIDEV with differential steering, the trajectory tracking multi-objective control method is studied. The dynamics model of the four-in-wheel motor independent-drive vehicle (4MIDEV) is established comprehensively considering the differential steering dynamics characteristics, longitudinal dynamics characteristics, and lateral dynamics characteristics. Takagi Sugeno (T-S) fuzzy method is adopted to deal with the nonlinear and time-varying characteristics of the model parameters such as vehicle longitudinal speed and the front steering wheel angle. The trajectory tracking control targets are divided into the kinematic control target considering the trajectory tracking accuracy and the dynamics control target considering longitudinal speed tracking as well as lateral stability performance. The generalized H_2 norm and H_∞ norm are selected to constrain the kinematic control target and the dynamics control target respectively. The generalized H_2/H_∞ trajectory tracking controller is designed to improve the trajectory tracking accuracy and longitudinal speed tracking as well as lateral stability performance. The hardware in the loop test (HIL) verified that the designed trajectory tracking multi-objective controller can improve the comprehensive performance of vehicle and balance the trajectory tracking accuracy between the longitudinal and lateral dynamics performance.

INDEX TERMS Differential steering, four-in-wheel-motor drive vehicle, multi-objective control, trajectory tracking, T-S fuzzy.

I. INTRODUCTION

The four-in-wheel-motor independent-drive vehicle (4MIDEV) have the advantages of rapid torque response and flexible control, which has been studied widely and shown great potential in the vehicle active safety control, stability control and intelligent driving control [1], [2]. The 4MIDEV eliminates the traditional mechanical transmission system, differential mechanism and transmission, and the four-wheel torques are controllable independently. Under the action of the steering trapezoid mechanism, the torque difference between the left and right front-wheels is generated, so as to achieve differential steering [3], [4].

The associate editor coordinating the review of this manuscript and approving it for publication was Jie Gao.

The trajectory tracking control for 4MIDEV was realized in [5] by coordinating the active front wheel steering (AFS) and the differential steering. The Steer-by-Wire (SBW) system and the differential steering system were both taken as the actuators of the trajectory tracking control for 4MIDEV in [6], and the trajectory tracking control was achieved by designing the coordination control strategy of SBW and differential steering. However, the in-wheel motors drive vehicle with active steering mechanism is a typical overdrive system. The increase of the number of actuators leads to more complexity and higher failure probability of the system [2], which will have an impact on the reliability and stability of the control system so that affecting the driving safety. Taking differential steering as an independent steering actuator without relying on any other steering mechanism will simplify the complexity of the system and reduce the probability of

actuator failure. Tian *et al.* designed a sliding mode controller based on differential steering dynamics model and the feasibility of the differential steering as the independent steering mechanism was verified therein [7]. Thus, it is particularly important to study the trajectory tracking control of differential steering as an independent steering mechanism.

There are some problems when taking the differential steering as an independent steering actuator. One of the problems is that the left-front and right-front wheel torque difference required for differential steering will generate additional yaw moments to vehicle, which will affect the lateral stability [8]. The differential steering dynamics characteristics and vehicle lateral dynamics characteristics were analyzed in [9], [10], and the dynamics model of 4MIDEV including differential steering dynamics characteristics was established. For the lateral stability problem of vehicle during differential steering process, the integrated sliding mode controller was designed in [4] to improve the vehicle's lateral stability performance, and the adaptive super-twisting method was used to suppress the chattering of sliding mode controller. The influence of the torque difference between the left-front and right-front wheels on the yaw rate was considered in [11], and the μ analysis theory was adopted to optimize yaw rate, so that it could better track the desired yaw rate. The 4MIDEV dynamics models established in these studies only included the lateral dynamics, but not the longitudinal dynamics. However, there is a strong coupling phenomenon between the longitudinal and lateral dynamics of vehicle, i.e. the longitudinal speed will be affected when vehicle performs differential steering [12], [13].

In order to solve this problem in the field of traditional vehicle, the coupling characteristics between longitudinal and lateral motion was considered in [14], a three-degree-of-freedom (3DOF) vehicle dynamic model including vehicle longitudinal motion, lateral motion and yaw motion was adopted to achieve the intelligent vehicle longitudinal and lateral motion control, and a relatively ideal control effect was achieved. Jin *et al.* [15] used 3DOF model including longitudinal dynamics characteristics to realize vehicle lateral stability control, and the vehicle stability was improved through the coordinated control of AFS and direct yaw moment. The 3DOF model mentioned above is not adapted to the control of 4MIDEV with differential steering due to the different steering principle between the differential steering and traditional steering system. The influence of differential steering on vehicle longitudinal and lateral dynamics are considered comprehensively in the process of trajectory tracking in this paper, and the dynamics model of 4MIDEV with differential steering is established by combining the differential steering dynamics equation, the vehicle longitudinal dynamics equation and the vehicle lateral dynamics equation. Compared with the traditional linear two-degree-of-freedom model which only considers the lateral motion and the yaw motion, the nonlinearity of the dynamics model of 4MIDEV with differential steering is greatly increased. Meanwhile, there are nonlinear time-varying parameters in this model, which increases the difficulty of the controller design. Takagi-Sugeno (T-S) fuzzy method has the advantages in dealing with the problems of model nonlinearity and parameters time-varying characteristics [15]–[18]. The T-S fuzzy method is used to deal with the nonlinear variation of the tire nonlinearity in the model in [15], and was adopted to deal with the nonlinearity variation of the vehicle longitudinal speed in [18]. However, when there are many time-varying parameters, the traditional T-S fuzzy method has the problem of large amount of numerical calculation.

In the research field of trajectory tracking control, Ji *et al.* considered the trajectory tracking accuracy and the lateral stability, and the game theory was adopted to deal with the contradiction between trajectory tracking accuracy and lateral stability [19]. Yuan *et al.* [20] adopted model predictive control method to design the trajectory tracking controller. The lane centerline tracking accuracy and the vehicle longitudinal dynamics characteristics were considered comprehensively in [21], and the model predictive control algorithm was used to design the controller, which enable vehicle to track the lane centerline and the desired longitudinal speed. Few studies have considered the trajectory tracking accuracy, lateral stability and longitudinal speed tracking performance comprehensively. For 4MIDEV with differential steering, if the longitudinal dynamics is not considered, speed fluctuation caused by differential steering during the trajectory tracking process will affect vehicle ride comfort. If the lateral stability is not considered, lateral stability will be affected by differential steering under the high speed or high curvature road so that the driving safety is affected. Therefore, it is necessary to consider the trajectory tracking accuracy, lateral stability and longitudinal speed tracking performance comprehensively in the meantime enhance the comprehensive performance of 4MIDEV trajectory tracking control system.

Common trajectory tracking control algorithms of intelligent vehicle include PID, LQR, MPC, sliding mode variable structure control and pure tracking control, and these methods are also mostly used in the research of 4MIDEV trajectory tracking. Li *et al.* [22] proposed a new potential field method based on yaw angle control to realize 4MIDEV trajectory tracking. The potential field method included attractive potential function, repulsive potential function, and yaw angle potential function, in which the purpose of yaw angle potential function was to reduce yaw angle rate change and improve the vehicle handling stability. The desired vehicle longitudinal force, lateral force, and yaw moment were determined according to the desired yaw angle and the desired longitudinal speed. Guo *et al.* [23] designed a trajectory tracking controller based on MPC in the upper layer, in the middle layer the fuzzy theory was used to optimize the parameters of proportional integral (PI) controller, and the additional yaw control torque was generated by sliding mode control (SMC). Hang *et al.* [24] designed a trajectory tracking controller for 4MIDEV based on MPC. At different speeds, the desired trajectory could be tracked well, but the desired yaw rate and longitudinal speed were not considered. Zheng and Yang [25]

designed a 4MIDEV trajectory tracking strategy based on Neural Network PID and SMC was used to track the desired yaw rate. The trajectory tracking controller based on Fuzzy Adaptive PID control algorithm was used in [26], however, PID controller was sensitive to parameter changes and was not suitable for nonlinear systems. Over the years, 4MIDEV trajectory tracking control method mainly faces the following problems. Firstly, there are few studies on comprehensively considering the track tracking accuracy, longitudinal speed tracking performance and lateral stability of 4MIDEV. Secondly, most of studies are carried out under the assumption of vehicle with the constant longitudinal speed, but it is important for 4MIDEV to control longitudinal speed, and we hope to track the trajectory with a high vehicle speed without losing vehicle stability, in addition the current longitudinal control method for intelligent vehicles is not suitable for 4MIDEV. The sliding mode variable structure controller was designed to track the desired vehicle longitudinal speed based on the longitudinal dynamic characteristics, the model predictive controller was designed to ensure the trajectory tracking accuracy in [27], and the direct yaw moment control was adopted to ensure the vehicle lateral stability when tracking the trajectory. Those three controllers were designed for trajectory tracking accuracy, vehicle lateral stability and vehicle longitudinal speed tracking performance respectively, which increased the complexity of the control system. Besides, there are certain coupling relationships between the different controllers, which had an impact on the comprehensive performance of the control system. So, it is expected to design one comprehensive controller to achieve multi control objectives, which can avoid the interaction among multiple controllers, reduce the complexity of the control system, and track the trajectory with a high vehicle speed without losing vehicle stability.

Based on the multi-objective control architecture, two or more dependent control objectives are transformed into linear matrix inequalities, and the solution of the multi-objective problem is obtained by solving the convex optimization problem, thus a single controller can be obtained to satisfy multiple control objectives [28]. The H_2 and generalized H_2 norms were used as the system performance indexes in [29], and multi-objective controller of active suspension system was designed to improve ride comfort and handling stability performances. Jin *et al.* [30] designed a robust H_∞ feedback controller for the closed-loop active suspension system. The H_2/H_∞ robust multi-objective controller was designed in [31] to enable the aircraft to better track the desired speed and desired attitude angle. At present, the multi-objective control method based on above mentioned multi-objective control architecture is widely used in aircraft attitude control, vehicle suspension control and mobile robot motion control, but less used in vehicle trajectory tracking control. Compared with wheeled mobile robot, the trajectory tracking accuracy should not only be considered, but also the vehicle dynamic performance should be focused on in the process of vehicle trajectory tracking control. In particular, 4MIDEV is a strong nonlinear redundant control system. The multi-objective control method can convert the trajectory tracking accuracy and dynamics performance into the convex optimization problem for solving the linear matrix inequalities, and then the solution of the multi-objective controller can be calculated. It is of great significance to apply the multi-objective control method based on the mentioned multi-objective control architecture for achieving the trajectory tracking control of 4MIDEV.

The main contribution of this paper is that the influences of the differential steering on vehicle longitudinal and lateral dynamics characteristics are considered. Furthermore, the dynamics model of 4MIDEV with differential steering is established by combining the differential steering dynamics characteristics, the vehicle longitudinal and lateral dynamics characteristics. Different from references [15] and [16], the T-S fuzzy method after first-order Taylor approximation is adopted to deal with the nonlinear model. The high trajectory tracking accuracy, good longitudinal speed tracking performance, and excellent lateral stability performance are taken as the control objectives in this paper. The above control objectives are divided into the kinematics index considering trajectory tracking accuracy and the dynamics index considering the vehicle longitudinal as well as lateral dynamics characteristics. Based on the multi-objective control architecture, the generalized H_2/H_∞ multi-objective controller is designed, and hardware in the loop test (HIL) is finally adopted to verify the effect of the designed control system.

The remaining sections of this paper are organized as follows. Vehicle dynamics model and the trajectory tracking model are established in section II, and the nonlinear state equation expression of the control system is obtained. The T-S fuzzy method is adopted to deal with the nonlinearity of the state equation in section III. Then, the control output parameters and the measurement output parameters are selected, and the system's T-S model is obtained. In section IV, the control targets are divided, and the generalized H_2/H_∞ norm are selected to design the multi-objective controller. The solution of the multi-objective controller is obtained by the steps of matrix block processing, linear variable replacement, convex optimization solution and the matrix singular value decomposition. In section V, the torque optimal distribution scheme is designed. HIL test is adopted to verify the effectiveness of the designed control systemin section VI. The section VII is the conclusion.

II. VEHICLE NONLINEAR DYNAMICS

A. DYNAMICS MODEL WITH DIFFERENTIAL STEERING

According to the differential steering principle of 4MIDEV in [4], the following dynamics equation of differential steering is built [4], [10].

$$\dot{\delta} = -\frac{l^2 C_f}{3b_e}\delta + \frac{k_1 C_f}{b_e}\beta + \frac{k_1 C_f l_f}{v_x b_e}\omega + \frac{r_\sigma}{b_e r}u_1 \qquad (1)$$

where b_e is the steering damping, r_σ is the distance between the projection point of the kingpin on the ground and the center plane of the tire, δ is the steering angle of front wheel,

β is the centroid sideslip angle, ω is the yaw rate, u_1 is the torque difference between two front wheels.

Ignoring the pitch and roll motion, the 4MIDEV dynamics model with the front-wheel differential steering is shown in Fig. 1.

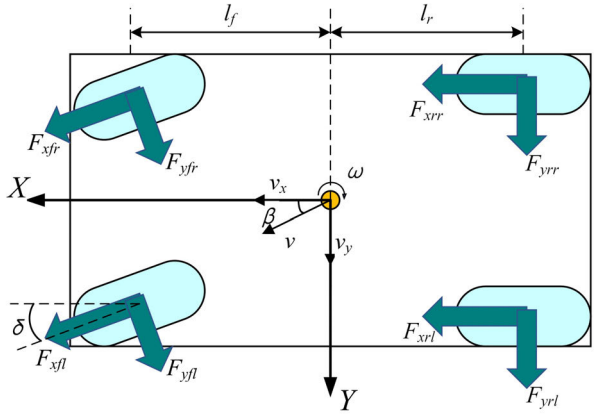

FIGURE 1. Framework of the 4MIDEV model.

The 3-DOF 4MIDEV dynamics model containing the vehicle longitudinal motion, lateral motion and yaw motion is built as follows [32].

$$\begin{cases} m\left(\dot{v}_x - v_y\omega\right) = \left(F_{xfl} + F_{xfr}\right)cos\delta + F_{xrl} + F_{xrr} \\ \qquad - \left(F_{yfl} + F_{yfr}\right)sin\delta \\ m\left(\dot{v}_y + v_x\omega\right) = \left(F_{yfl} + F_{yfr}\right)cos\delta + F_{yrl} + F_{yrr} \\ \qquad + \left(F_{xfl} + F_{xfr}\right)sin\delta \\ I_z\dot{\omega} = l_f\left(F_{yfl} + F_{yfr}\right)cos\delta - l_r\left(F_{yrl} + F_{yrr}\right) \\ \qquad + l_f\left(F_{xfl} + F_{xfr}\right)sin\delta \end{cases} \tag{2}$$

where m is the mass of the whole vehicle, v_x and v_y are the longitudinal speed and the lateral speed respectively, l_f and l_r are the distances from the mass center of vehicle to the front and rear axles respectively, I_z is the vehicle moment of inertia around z-axle, fl, fr, rl and rr represent the left-front wheel, right-front wheel, left-rear wheel and right-rear wheel respectively. Let $i = fl, fr, rl, rr$, and F_{xi}, F_{yi} indicate the longitudinal forces and lateral forces of tires respectively.

When the differential steering occurs, the lateral force and longitudinal force of tires will become to change [4], [32]. According to (2), the longitudinal acceleration is affected by the change of the lateral or longitudinal force. Therefore, differential steering affects the vehicle longitudinal dynamic performance.

Let $F_{yi} = C_i\alpha_i$, where C_i is the cornering stiffness of tires and α_i is the centroid sideslip angle of tires. In order to simplify the model, assuming that $C_{fl} = C_{fr}, C_{rl} = C_{rr}$, $\alpha_{fl} = \alpha_{fr}, \alpha_{rl} = \alpha_{rr}$, and $C_f = C_{fl} + C_{fr}, C_r = C_{rl} + C_{rr}$, $\alpha_f = \alpha_{fl} = \alpha_{fr}, \alpha_r = \alpha_{rl} = \alpha_{rr}$. By introducing additional yaw moment u_2 and the driving torque u_3, the following vehicle dynamics model with differential steering can be obtained according to the differential steering dynamics shown in (1).

$$\begin{cases} \dot{\delta} = -\frac{k_1C_f}{b_e}\delta + \frac{k_1C_f}{b_e}\beta + \frac{k_1C_fl_f}{v_xb_e}\omega + \frac{r_\sigma}{b_er}u_1 \\ \dot{v}_x = \frac{C_fsin\delta}{m}\delta + \left(v_y - \frac{C_fl_fsin\delta}{mv_x}\right)\omega - \frac{C_fsin\delta}{m}\beta \\ \qquad + \frac{1+cos\delta}{2mr}u_3 \\ \dot{\beta} = -\frac{C_fcos\delta}{mv_x}\delta + \left(\frac{C_fl_fcos\delta - C_rl_r}{mv_x^2} - 1\right)\omega + \frac{C_fcos\delta + C_r}{mv_x}\beta \\ \qquad + \frac{sin\delta}{2mv_xr}u_3 \\ \dot{\omega} = -\frac{C_fl_fcos\delta}{I_z}\delta + \frac{C_fl_f^2cos\delta + C_rl_r^2}{I_zv_x}\omega + \frac{C_fl_fcos\delta - C_rl_r}{I_z}\beta \\ \qquad + \frac{l_s}{I_zr}u_1 + \frac{1}{I_z}u_2 + \frac{l_fsin\delta}{2I_zr}u_3 \end{cases} \tag{3}$$

where r is effective rolling radius of the wheels.

B. IN-WHEEL MOTOR MODEL

The permanent magnet synchronous outer rotor motor is selected as in-wheel motor due to its characteristics of high efficiency, rapid torque response, and being easy to connect with the hub directly. The permanent magnet synchronous outer rotor motor can be simplified as a second-order system [33]. The equation of motor is expressed as follows.

$$\frac{T_{\mathrm{mi}}}{T_{\mathrm{wi}}} = \frac{1}{2\xi^2s^2 + 2\xi s + 1} \tag{4}$$

where ξ is determined by electromagnetic parameters of motor and set as 0.05, T_{mi} is output torque of the motor, T_{wi} is the target motor torque. The motor's rated power is 5 kw, the peak torque is 200 N · m, the peak speed is 780 r/min, and the rated voltage is 72 V.

C. TRAJECTORY TRACKING MODEL

The trajectory tracking model is shown in Fig. 2, where e is the lateral deviation, ρ is the road curvature, ψ_h is the vehicle's actual heading angle, ψ_d is the desired heading angle, and the heading angle deviation $\psi = \psi_h - \psi_d$. The equation of the trajectory tracking is expressed as follows [10], [34].

$$\begin{cases} \dot{e} = v_x\psi + v_x\beta \\ \dot{\psi} = \omega - \rho v_x \end{cases} \tag{5}$$

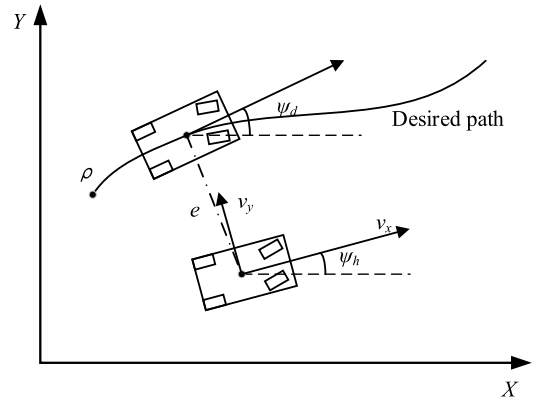

FIGURE 2. Trajectory tracking model.

D. STATE EQUATION EXPRESSION

The following time-varying state equation is obtained by combining the above models. There are some time-varying parameters such as vehicle longitudinal speed v_x, lateral speed v_y, and the front wheel steering angle δ in the coefficient matrixes of the state equation.

$$\dot{X} = A(t)X + B(t)U + B_1(t)W \tag{6}$$

where ω_d is desired yaw rate, $\omega_d = \min\{\omega_{d1}, \omega_{lim}\} * sgn(\delta)$, $\omega_{lim} = \frac{0.85}{v_x}\mu g$, $\omega_{d1} = \frac{v_x/L}{1+Kv_x^2}\sigma$, K is the stability factor, v_{xd} is the desired longitudinal speed, X is the state vector, U is the control output vector, W is the external disturbance vector, μ is the friction coefficient of the road surface, l_s is the half of the wheel-base, and k_1, k_2, k_3 are weighting coefficients.

$$A(t) = \begin{bmatrix} 0 & v_x(t) & 0 & 0 & v_x(t) & 0 \\ 0 & 0 & 0 & 0 & 0 & 1 \\ 0 & 0 & -o_1 & 0 & o_1 & \frac{o_1 l_f}{v_x(t)} \\ 0 & 0 & o_2 & 0 & -o_2 & v_y(t) - \frac{o_2 l_f}{v_x(t)} \\ 0 & 0 & -o_3 & 0 & \frac{C_r}{m v_x(t)} + o_3 & \frac{o_3 l_f}{v_x(t)} - \frac{C_r l_r}{m(v_x(t))^2} - 1 \\ 0 & 0 & -o_4 & 0 & o_4 - \frac{C_r l_r}{I_z} & \frac{o_4 l_f}{v_x(t)} + \frac{C_r l_r^2}{I_z v_x(t)} \end{bmatrix},$$

$$B_1(t) = \begin{bmatrix} 0 & 0 & 0 \\ -\frac{v_x(t)}{k_1} & 0 & 0 \\ 0 & 0 & 0 \\ 0 & 0 & 0 \\ 0 & 0 & 0 \\ 0 & 0 & 0 \end{bmatrix}, B(t) = \begin{bmatrix} 0 & 0 & 0 \\ 0 & 0 & 0 \\ \frac{r_\sigma}{b_e r} & 0 & 0 \\ 0 & 0 & \frac{1+\cos(\delta(t))}{2mr} \\ 0 & 0 & \frac{\sin(\delta(t))}{2mrv_x(t)} \\ \frac{l_s}{I_z r} & \frac{1}{I_z} & \frac{l_f \sin(\delta(t))}{2I_z r} \end{bmatrix}.$$

$$X = [e\ \psi\ \delta\ v_x\ \beta\ \omega]^T,\ U = [u_1\ u_2\ u_3]^T,$$
$$W = [k_1\rho\ k_2 v_{xd}\ k_3\omega_d]^T.$$
$$o_1 = \frac{k_1 C_f}{b_e}, o_2 = \frac{C_f \sin(\delta(t))}{m}, o_3 = \frac{C_f \cos(\delta(t))}{m v_x(t)},$$
$$o_4 = \frac{C_f l_f \cos(\delta(t))}{I_z}.$$

III. SYSTEM MODEL ESTABLISHMENT WITH T-S FUZZY METHOD

A. T-S FUZZY STATE EQUATION

As vehicle driving condition changes, the parameters in coefficient matrixes $A(t)$, $B(t)$, $B_1(t)$ such as $v_x(t)$, $v_y(t)$, and $\delta(t)$ will change with the time nonlinearly, that is to say, the coefficient matrixes of the state equation change with the change of time-varying parameters $v_x(t)$, $v_y(t)$, $\delta(t)$, which will bring difficulty to the multi-objective controller designing. Due to the effectiveness of the T-S fuzzy method in dealing with the model nonlinear problem [15], [18], the T-S fuzzy method is adopted to deal with the nonlinear time-varying parameters in (6) to obtain the linearized state equation expression.

$v_x(t)$, $v_y(t)$, and $\delta(t)$ can be obtained by the method of measurement or estimation [35], and these three parameters are bounded in the actual vehicle driving process. Let $\max v_x = \overline{v_x}$, $\min v_x = \widetilde{v_x}$, $\max v_y = \overline{v_y}$, $\min v_y = \widetilde{v_y}$, $\max\delta =, \min\delta = \widetilde{\delta}$. If v_x, $1/v_x$, $1/v_x^2$, $sin\delta$, $cos\delta$, v_y are selected as the premise variables, and each premise variable is divided into two fuzzy sets of "high" and "low". Thus, a total of 2^6 fuzzy rules are obtained, which makes the numerical calculation of the obtained global linearization system state equation larger, and have a great impact on the controller's real time performance [36]. In order to reduce the numerical calculation, the premise variables $1/v_x$, $1/v_x^2$, $sin\delta$, $\cos\delta$ are processed by using the first-order Taylor approximation method.

Firstly, the premise variables $1/v_x$ and $1/v_x^2$ are processed by the method of the first-order Taylor approximation at the point of $v_0 = (\overline{v_x} + \widetilde{v_x})/2$.

$$\frac{1}{v_x} \approx \frac{1}{v_0} - \frac{1}{v_0^2}(v_x - v_0), \frac{1}{v_x^2} \approx \frac{1}{v_0^2} - \frac{2}{v_0^3}(v_x - v_0) \tag{7}$$

The premise variables $\sin\delta$ and $\cos\delta$ are processed by the method of the first-order Taylor approximation at the point of $\delta_0 = \frac{\delta_{max}+\delta_{min}}{2}$. We get

$$sin\delta \approx \delta, cos\delta \approx 1 \tag{8}$$

The number of premise variables are correspondingly reduced to three by substituting (7) and (8) into (6), and the premise variables are rewritten as $\rho_1(t) = v_x$, $\rho_2(t) = v_y$, $\rho_3(t) = \delta$. Each premise variable here is divided into two fuzzy sets of "high" and "low", a total of 2^3 fuzzy rules are obtained. According to [21], the $\widetilde{v_x} = 10$m/s, $\overline{v_x} = 30$m/s, $\widetilde{v_y} = -6$m/s, $\overline{v_y} = 6$m/s are set in this paper. According to the general range of front wheel steering angle, $\widetilde{\delta} = -\pi/6$ rad and $\bar{\delta} = \pi/6$ rad are selected in this paper.

For the premise variables $\rho_1(t)$, $\rho_2(t)$, $\rho_3(t)$ the membership functions are calculated as follows [37].

$$M_1^1(\rho_1(t)) = \frac{v_x - \widetilde{v_x}}{\overline{v_x} - \widetilde{v_x}}, M_1^2(\rho_1(t)) = \frac{\overline{v_x} - v_x}{\overline{v_x} - \widetilde{v_x}}$$
$$M_2^1(\rho_2(t)) = \frac{v_y - \widetilde{v_y}}{\overline{v_y} - \widetilde{v_y}}, M_2^2(\rho_2(t)) = \frac{\overline{v_y} - v_y}{\overline{v_y} - \widetilde{v_y}}$$
$$M_3^1(\rho_3(t)) = \frac{\delta - \widetilde{\delta}}{\bar{\delta} - \widetilde{\delta}}, M_3^2(\rho_3(t)) = \frac{\bar{\delta} - \widetilde{\delta}}{\bar{\delta} - \widetilde{\delta}}$$

The following T-S fuzzy state equation is obtained.

$$\dot{X} = \sum_{i=1}^{8} \overline{\mu_i}(A_i X + B_i U + B_{1i} W) \tag{9}$$

where $\overline{\mu_i} = \frac{\mu_i}{\sum_{i=1}^{8}\mu_i}$, $\mu_i = \prod_{j=1}^{3} M_j^k$, M_j^k is the degree of the membership of the j_{th} rule, $k = 1, 2$. The rules are as follows.

If $\rho_1(t)$ is "low", $\rho_2(t)$ is "low", $\rho_3(t)$ is "low", then $\dot{X} = A_1 X + B_1 U + B_{11} W$,

If $\rho_1(t)$ is "high", $\rho_2(t)$ is "low", $\rho_3(t)$ is "low", then $\dot{X} = A_2 X + B_2 U + B_{12} W$,

$\vdots$

If $\rho_1(t)$ is "high", $\rho_2(t)$ is "high", $\rho_3(t)$ is "high", then $\dot{X} = A_8 X + B_8 U + B_{18} W$, where $A_1, B_1, A_2, B_2, \cdots A_8, B_8$, are shown at the bottom of the next page

$$A_1 = \begin{bmatrix} 0 & \widetilde{v_x} & 0 & 0 & \widetilde{v_x} & 0 \\ 0 & 0 & 0 & 0 & 0 & 1 \\ 0 & 0 & -\frac{k_1 C_f}{b_e} & 0 & \frac{k_1 C_f}{b_e} & \frac{2k_1 C_f l_f}{v_0 b_e} - \frac{k_1 C_f l_f \widetilde{v_x}}{b_e v_0^2} \\ 0 & 0 & \frac{C_f \widetilde{\delta}}{m} & 0 & -\frac{C_f \widetilde{\delta}}{m} & \widetilde{v_y} - \frac{2C_f l_f \widetilde{\delta}}{m v_0} + \frac{C_f l_f \widetilde{v_x} \widetilde{\delta}}{m v_0^2} \\ 0 & 0 & -\frac{2C_f}{m v_0} + \frac{C_f \widetilde{v_x}}{m v_0^2} & 0 & \frac{2(C_r + C_f)}{m v_0} - \frac{\widetilde{v_x}(C_f + C_r)}{m v_0^2} & \frac{3(C_f l_f - C_r l_r)}{m v_0^2} - \frac{2\widetilde{v_x}(C_f l_f - C_r l_r)}{m v_0^3} - 1 \\ 0 & 0 & -\frac{C_f l_f}{I_z} & 0 & \frac{C_f l_f - C_r l_r}{I_z} & \frac{(C_f l_f^2 + C_r l_r^2)(2v_0 - \widetilde{v_x})}{I_z v_0^2} \end{bmatrix},$$

$$B_1 = \begin{bmatrix} 0 & 0 & 0 \\ 0 & 0 & 0 \\ \frac{r_\sigma}{b_e r} & 0 & 0 \\ 0 & 0 & \frac{1}{mr} \\ 0 & 0 & \frac{\widetilde{\delta}}{m v_0 r} - \frac{\widetilde{\delta} \widetilde{v_x}}{2mr v_0^2} \\ \frac{l_s}{I_z r} & \frac{1}{I_z} & \frac{l_f \widetilde{\delta}}{2 I_z r} \end{bmatrix}, B_{11} = \begin{bmatrix} 0 & 0 \\ -\widetilde{v_x} & 0 \\ 0 & 0 \\ 0 & 0 \\ 0 & 0 \\ 0 & 0 \end{bmatrix}.$$

$$A_2 = \begin{bmatrix} 0 & \overline{v_x} & 0 & 0 & \overline{v_x} & 0 \\ 0 & 0 & 0 & 0 & 0 & 1 \\ 0 & 0 & -\frac{k_1 C_f}{b_e} & 0 & \frac{k_1 C_f}{b_e} & \frac{2k_1 C_f l_f}{v_0 b_e} - \frac{k_1 C_f l_f \overline{v_x}}{b_e v_0^2} \\ 0 & 0 & \frac{C_f \widetilde{\delta}}{m} & 0 & -\frac{C_f \widetilde{\delta}}{m} & \widetilde{v_y} - \frac{2C_f l_f \widetilde{\delta}}{m v_0} + \frac{C_f l_f \overline{v_x} \widetilde{\delta}}{m v_0^2} \\ 0 & 0 & -\frac{2C_f}{m v_0} + \frac{C_f \overline{v_x}}{m v_0^2} & 0 & \frac{2(C_r + C_f)}{m v_0} - \frac{\overline{v_x}(C_f + C_r)}{m v_0^2} & \frac{3(C_f l_f - C_r l_r)}{m v_0^2} - \frac{2\overline{v_x}(C_f l_f - C_r l_r)}{m v_0^3} - 1 \\ 0 & 0 & -\frac{C_f l_f}{I_z} & 0 & \frac{C_f l_f - C_r l_r}{I_z} & \frac{(C_f l_f^2 + C_r l_r^2)(2v_0 - \overline{v_x})}{I_z v_0^2} \end{bmatrix},$$

$$B_2 = \begin{bmatrix} 0 & 0 & 0 \\ 0 & 0 & 0 \\ \frac{r_\sigma}{b_e r} & 0 & 0 \\ 0 & 0 & \frac{1}{mr} \\ 0 & 0 & \frac{\widetilde{\delta}}{m v_0 r} - \frac{\widetilde{\delta} \overline{v_x}}{2mr v_0^2} \\ \frac{l_s}{I_z r} & \frac{1}{I_z} & \frac{l_f \widetilde{\delta}}{2 I_z r} \end{bmatrix}, B_{12} = \begin{bmatrix} 0 & 0 \\ -\overline{v_x} & 0 \\ 0 & 0 \\ 0 & 0 \\ 0 & 0 \\ 0 & 0 \end{bmatrix}.$$

$$\vdots$$

$$A_8 = \begin{bmatrix} 0 & \overline{v_x} & 0 & 0 & \overline{v_x} & 0 \\ 0 & 0 & 0 & 0 & 0 & 1 \\ 0 & 0 & -\frac{k_1 C_f}{b_e} & 0 & \frac{k_1 C_f}{b_e} & \frac{2k_1 C_f l_f}{v_0 b_e} - \frac{k_1 C_f l_f \overline{v_x}}{b_e v_0^2} \\ 0 & 0 & \frac{C_f \bar{\delta}}{m} & 0 & -\frac{C_f \bar{\delta}}{m} & \overline{v_y} - \frac{2C_f l_f \bar{\delta}}{m v_0} + \frac{C_f l_f \overline{v_x} \bar{\delta}}{m v_0^2} \\ 0 & 0 & -\frac{2C_f}{m v_0} + \frac{C_f \overline{v_x}}{m v_0^2} & 0 & \frac{2(C_r + C_f)}{m v_0} - \frac{\overline{v_x}(C_f + C_r)}{m v_0^2} & \frac{3(C_f l_f - C_r l_r)}{m v_0^2} - \frac{2\overline{v_x}(C_f l_f - C_r l_r)}{m v_0^3} - 1 \\ 0 & 0 & -\frac{C_f l_f}{I_z} & 0 & \frac{C_f l_f - C_r l_r}{I_z} & \frac{(C_f l_f^2 + C_r l_r^2)(2v_0 - \overline{v_x})}{I_z v_0^2} \end{bmatrix},$$

$$B_8 = \begin{bmatrix} 0 & 0 & 0 \\ 0 & 0 & 0 \\ \frac{r_\sigma}{b_e r} & 0 & 0 \\ 0 & 0 & \frac{1}{mr} \\ 0 & 0 & \frac{\bar{\delta}}{m v_0 r} - \frac{\bar{\delta} \overline{v_x}}{2mr v_0^2} \\ \frac{l_s}{I_z r} & \frac{1}{I_z} & \frac{l_f \bar{\delta}}{2 I_z r} \end{bmatrix}, B_{18} = \begin{bmatrix} 0 & 0 \\ -\overline{v_x} & 0 \\ 0 & 0 \\ 0 & 0 \\ 0 & 0 \\ 0 & 0 \end{bmatrix}.$$

B. OUTPUT SELECTION OF THE SYSTEM WITH T-S FUZZY MODEL

The trajectory tracking control of 4MIDEV is studied in this paper. Therefore, one of the control objectives is to ensure the trajectory tracking accuracy. Since the differential steering is used as the actuator of trajectory tracking, the torque difference between the left and right front wheels required by differential steering will introduce additional yaw moment, which will affect the lateral stability of the vehicle. At the same time, the vehicle has strong longitudinal and lateral coupling dynamics characteristics. In the process of trajectory tracking, the differential steering will have an impact on the vehicle's longitudinal dynamics characteristics, and one of the intuitive performances is the influence of the differential steering on the longitudinal vehicle speed. Therefore, high trajectory tracking accuracy, good desired longitudinal speed tracking and lateral stability performance are taken as the comprehensive control objectives in this paper. The lateral deviation e and the heading angle deviation ψ are selected to describe the trajectory tracking accuracy [22], [38], the yaw rate ω and the centroid sideslip angle β are selected to describe the vehicle lateral stability performance [39], [40], and the vehicle longitudinal speed v_x is selected to describe the longitudinal speed tracking performance [13], [21].

It is noted that the two variables e and ψ, which indicate the trajectory tracking accuracy, are the variables describing the geometric relationship between the vehicle and the desired trajectory, and belong to the vehicle kinematic category; while the variables ω, β, v_x, which indicate the vehicle lateral stability and longitudinal dynamics characteristics, are closely related to the vehicle's forces relationship and belong to the vehicle dynamics category. Therefore, the trajectory tracking control of 4MIDEV is not only a multi-objective control problem, but also a kinematics and dynamics integration problem. The control outputs are divided into kinematic control output $Z_1 = [k_8 e \;\; k_9\psi]^T$ and the dynamics control output $Z_2 = [k_4\dot{e}_1 \;\; k_5\dot{e}_2 \;\; k_6\dot{e}_3 \;\; k_7\beta]^T$, and the measurement output $Y = [e \;\; \psi \;\; \dot{e}_1 \;\; \dot{e}_2 \;\; \dot{e}_3]^T$ is also selected, where $\dot{e}_1 = \delta - \delta_d$, $\dot{e}_2 = v_x - v_{xd}$ and $\dot{e}_3 = \omega - \omega_d$. The parameters $k_4, k_5, \ldots, k_9$ are the weighting coefficients.

By combining (9), the following state space equation expression of the system's T-S fuzzy model is obtained.

$$\begin{cases} \dot{X} = \sum_{i=1}^{8} \overline{\mu}_i (A_i X + B_i U + B_{1i} W) \\ Z_1 = C_{11} X + D_{11} W \\ Z_2 = C_{12} X + D_{12} W \\ Y = CX + DW \end{cases} \tag{10}$$

where

$$C_{11} = \begin{bmatrix} k_8 & 0 & 0 & 0 & 0 & 0 \\ 0 & k_9 & 0 & 0 & 0 & 0 \end{bmatrix},$$

$$C_{12} = \begin{bmatrix} -\frac{2k_4L}{d^2} & -\frac{2k_4L}{d} & k_4 & 0 & 0 & 0 \\ 0 & 0 & 0 & k_5 & 0 & 0 \\ 0 & 0 & 0 & 0 & 0 & k_6 \\ 0 & 0 & 0 & 0 & k_7 & 0 \end{bmatrix},$$

$$D_{11} = \begin{bmatrix} 0 & 0 & 0 \\ 0 & 0 & 0 \end{bmatrix}, D_{12} = \begin{bmatrix} 0 & 0 & 0 \\ 0 & -\frac{k_5}{k_2} & 0 \\ 0 & 0 & -\frac{k_6}{k_3} \\ 0 & 0 & 0 \end{bmatrix},$$

$$C = \begin{bmatrix} 1 & 0 & 0 & 0 & 0 & 0 \\ 0 & 1 & 0 & 0 & 0 & 0 \\ -\frac{2L}{d^2} & -\frac{2L}{d} & 1 & 0 & 0 & 0 \\ 0 & 0 & 0 & 1 & 0 & 0 \\ 0 & 0 & 0 & 0 & 0 & 1 \end{bmatrix}, D = \begin{bmatrix} 0 & 0 & 0 \\ 0 & 0 & 0 \\ 0 & 0 & 0 \\ 0 & -\frac{1}{k_2} & 0 \\ 0 & 0 & -\frac{1}{k_3} \end{bmatrix}.$$

IV. MULTI-OBJECTIVE CONTROLLER DESIGN

In this section, the multi-objective trajectory tracking controller is designed based on output feedback method. The proposed multi-objective trajectory tracking control system is shown in Fig. 3. Firstly, the nonlinear dynamics equation of 4MIDEV is established by combining the vehicle dynamics model with differential steering, the in-wheel motor model, and trajectory tracking error model. Taking lateral deviation, longitudinal speed, yaw rate et al as the control objectives, the generalized H_2 norm and H_∞ norm are selected to constrain vehicle control objectives. Then the output feedback control law is designed based on the control objectives, and the closed-loop T-S fuzzy state equation is obtained by combining the output feedback control law with the T-S fuzzy model. Finally, the closed-loop T-S fuzzy state equations are transformed into the linear matrix inequalities (LMI). The solution of trajectory tracking output feedback controller is obtained by solving the system of linear matrix inequalities. Control signal outputted by the multi-objective controller are the torque difference between the left-front wheel and the right-front wheel, the additional yaw moment, and the driving torque. The torque allocation algorithm is then designed for 4MIDEV.

The parallel distributed compensation (PDC) method is adopted to design the multi-objective output feedback controller for the T-S fuzzy model obtained in the above section. The design of the multi-objective output feedback controller mainly includes two parts, which are control index selection and the output feedback control law design. Firstly, the generalized H_2 performance index and H_∞ performance index are designed for trajectory tracking accuracy, longitudinal speed tracking performance, and lateral stability respectively, the Lyapunov matrix is introduced to transform different performance index constraints into a matrix equation inequalities form. Then, the solution of the multi-objective controller is obtained by the steps of Lyapunov matrix block processing, linear variable replacement formula, convex optimization solution and matrix singular value decomposition.

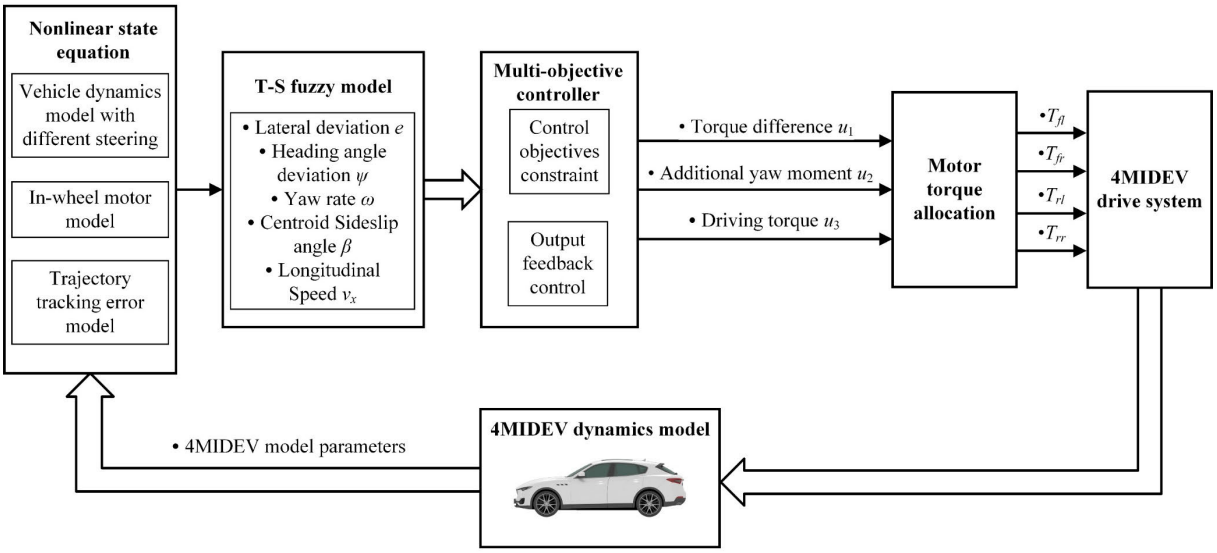

FIGURE 3. Multi-objective trajectory tracking control system framework.

A. CONTROL INDEX SELECTION

For the trajectory tracking accuracy, the variables e and ψ, which represent the geometric position relationship between 4MIDEV and the trajectory, needs to be as small as possible to ensure higher trajectory tracking accuracy. The transfer function from the external disturbance W to control output Z_1 is defined as T_1, then the generalized H_2 norm of the transfer function is defined as follows.

$$\|T_1\|_{GH2} = \sup_{W \in L_2} \frac{\|Z_1\|_\infty}{\|W\|_2} \tag{11}$$

where $\|Z_1\|_\infty = sup_{k \in N_0} |Z_1(k)|$ is the upper bound of the control output Z_1, $\|W\|_2 = \sqrt{\sum_{k=0}^{\infty} |W(k)|^2}$ is the square root value of the energy of the disturbance input signal, and $W \in L_2$ represents that the disturbance input signal W is the energy bounded signal. The generalized H_2 norm can describe the peak value of the control output in the time domain when the disturbance input signal is the energy bounded signal, that is to say, the generalized H_2 norm is a performance index which describes the hard constraint of the time domain output. Since the external disturbance signal W is studied in a limited time range, the external disturbance signal W is regarded as a bounded energy signal in this paper Therefore, the generalized H_2 norm is selected to perform the hard constraint for the variables e and ψ, so as to obtain higher trajectory tracking accuracy.

For the good longitudinal speed tracking performance and lateral stability, it is necessary to constrain the dynamics control output Z_2 to a small range to obtain a better dynamics response performance. At the same time, the vehicle dynamics response needs to be robust to the external disturbance such as the road curvature change. The transfer function from the external disturbance W to control output Z_2 is defined as T_2, then the H_∞ norm of the transfer function is defined as follows.

$$\|T_2\|_{GH2} = \sup_{W \in L_2} \frac{\|Z_2\|_\infty}{\|W\|_\infty} \tag{12}$$

where $\|Z_2\|_2 = \sqrt{\sum_{k=0}^{\infty} |Z_2(k)|^2}$ is the square root value of the energy of the control output signal Z_2. The H_∞ norm represents the peak value of the maximum singular value of the system frequency response, reflecting the energy ration of the system output signal to the input signal under the action of the energy bounded signal, which can describe the anti-disturbance performance from the external disturbance inputs to the control outputs. Therefore, the H_∞ norm index is adopted to ensure the vehicle's dynamics performances and the robustness of the vehicle dynamics responses.

B. OUTPUT FEEDBACK CONTROL LAW DESIGN

Considering that the relevant state variables such as the vehicle centroid sideslip angle and so on in the state feedback control are difficult to measure or the measuring cost is high, the output feedback control is adopted. The PDC method is used to design the output feedback control law for each local linear model of the T-S fuzzy system. A fuzzy global output feedback control law is finally obtained by the fuzzy synthesis of multiple local output feedback control laws. For a single local linear model, the output feedback control law is designed as follows.

$$U_i = K_i Y \tag{13}$$

The K_i in (13) has the following form.

$$\begin{cases} \dot{\hat{X}} = A_{ki}\hat{X} + B_{ki}Y \\ U = C_{ki}\hat{X} + D_{ki}Y \end{cases} \tag{14}$$

where A_{ki}, B_{ki}, C_{ki} and D_{ki} are the parameters matrixes of the controller.

The following closed-loop system is obtained by combining (10), (13) and (14).

$$\begin{cases} \dot{\xi} = A_{ci}\xi + B_{ci}W \\ Z_1 = C_{11}X + D_{11}W \\ Z_2 = C_{12}X + D_{12}W \end{cases} \tag{15}$$

where $A_{ci} = \begin{bmatrix} A_i + B_i D_{ki} C & B_i C_{ki} \\ B_{ki} C & A_{ki} \end{bmatrix}$, $B_{ci} = \begin{bmatrix} B_i D_{ki} D + B_{1i} \\ B_{ki} D \end{bmatrix}$, $\xi = \begin{bmatrix} X \\ \hat{X} \end{bmatrix}$.

The closed-loop system shown in (15) is required to be stable and the following conditions are required to be also met.

① $\|T_1\|_{GH2} < \lambda_1$

② $\|T_2\|_{\infty} < \lambda_2$

③ The poles of the closed-loop system are located in the left half open complex plane.

The sufficient and necessary condition for satisfying the condition ① is that there is a symmetric matrix $P_1 = P_1^T > 0$, which makes the following inequalities true.

$$\begin{pmatrix} A_{ci}^T P_1 + P_1 A_{ci} & P_1 B_{ci} \\ B_{ci}^T P_1 & -I \end{pmatrix} < 0 \tag{16}$$

$$\begin{pmatrix} P_1 & C_{11}^T \\ C_{11} & \lambda_1 I \end{pmatrix} > 0 \tag{17}$$

The sufficient and necessary condition for satisfying the condition ② is that there is a symmetric matrix $P_2 = P_2^T > 0$, which makes the following inequality true.

$$\begin{pmatrix} A_{ci}^T P_2 + P_2 A_{ci} & P_2 B_{ci} & C_{12}^T \\ B_{ci}^T P_2 & -\lambda_2 I & D_{12}^T \\ C_{12} & D_{12} & -\lambda_2 I \end{pmatrix} < 0 \tag{18}$$

The sufficient and necessary condition for satisfying the condition ③ is that there is a symmetric matrix $P_3 = P_3^T > 0$, which makes the following inequality true.

$$A_{ci} P_3 + P_3 A_{ci}^T < 0 \tag{19}$$

Since three symmetric positive definite matrices P_1, P_2 and P_3 are introduced in (16)∼(19), it is difficult to apply the existing theory to simultaneously solve the matrices P_1, P_2 and P_3 satisfying the constraints. The Lyapunov matrix $P = P_1 = P_2 = P_3$ is introduced to simplify the above problem. It is worth noting that although the Lyapunov matrix will bring some conservatism to the controller solution, the unification of each channel Lyapunov function makes the multi-objective controller design more flexible than the traditional optimal design, and it can reduce the order of the controller.

Then, the above constraint problem is converted into following form.

$$\begin{cases} \begin{pmatrix} A_{ci}^T P + P A_{ci} & P B_{ci} \\ B_{ci}^T P & -I \end{pmatrix} < 0 \\ \begin{pmatrix} P & C_{11}^T \\ C_{11} & \lambda_1 I \end{pmatrix} > 0 \\ \begin{pmatrix} A_{ci}^T P + P A_{ci} & P B_{ci} & C_{12}^T \\ B_{ci}^T P & -\lambda_2 I & D_{12}^T \\ C_{12} & D_{12} & -\lambda_2 I \end{pmatrix} < 0 \\ A_{ci} P + P A_{ci}^T < 0 \end{cases} \tag{20}$$

Since A_{ci} and B_{ci} in (20) depend on the unknown controller parameters matrixes A_{ki}, B_{ki}, C_{ki} and D_{ki}, there are nonlinear relationship between the matrix P and the controller parameters matrixes A_{ki}, B_{ki}, C_{ki} and D_{ki}, which brings great difficulties to the design of output feedback controller. The matrix inequalities shown in (20) is transformed into an equivalent linear matrix inequality by using the variable replacement method to find a proper variable replacement formula.

The matrixes blocking process method is carried out for the matrix P and its inverse matrix. We get

$$P = \begin{bmatrix} S & N \\ N^T & T \end{bmatrix}, P^{-1} = \begin{bmatrix} R & M \\ M^T & V \end{bmatrix} \tag{21}$$

where $R, S \in R^{n \times n}$ are symmetric matrix. The matrixes F_1 and F_2 are defined as follows.

$$F_1 = \begin{bmatrix} R & I \\ M^T & 0 \end{bmatrix}, F_2 = \begin{bmatrix} I & S \\ 0 & N^T \end{bmatrix}, F_2 = P F_1 \tag{22}$$

The variable replacement formulas are defined as follows.

$$\begin{cases} \widehat{A}_i = S\left(A_i + B_i D_{ki} C\right) R + N B_{ki} C R \\ \qquad + S B_i C_{ki} M^T + N A_{ki} M^T \\ \widehat{B}_i = S B_i D_{ki} + N B_{ki} \\ \widehat{C}_i = D_{ki} C R + C_{ki} M^T \\ \widehat{D}_i = D_{ki} \end{cases} \tag{23}$$

According to (23), the first matrix inequality in (20) is left multiplied by the matrix $diag\left\{F_1^T, I_1\right\}$ and right multiplied by the matrix $diag\{F_1, I_1\}$ respectively; the second matrix inequality in (20) is left multiplied by the matrix $diag\left\{F_1^T, I_2\right\}$ and right multiplied by the matrix $diag\{F_1, I_2\}$ respectively; the third matrix inequality in (20) is left multiplied by the matrix $diag\left\{F_1^T, I_1, I_3\right\}$ and right multiplied by the matrix $diag\{F_1, I_1, I_3\}$ respectively; and the fourth matrix inequality in (20) is left multiplied by the matrix F_1^T and right multiplied by the matrix F_1 respectively. The following matrix inequalities are obtained.

Equation (24), as shown at the bottom of the next page, is a linear matrix inequality about the parameter matrixes $\widehat{A}_i$, $\widehat{B}_i$, $\widehat{C}_i$, $\widehat{D}_i$, R, S, and which can be solved by the method of the convex optimization solution using the MATLAB toolbox.

According to (21), we get

$$MN^T = I - RS \tag{25}$$

After the matrixes R and S are obtained, the full rank matrixes M and N can be obtained by singular value decomposition of the matrix $I - RS$, and the parameters matrixes of the controller can be obtained through the following formula.

$$\begin{cases} D_{ki} = \widehat{D}_i \\ C_{ki} = \left(\widehat{C}_i - D_{ki}CR\right)\left(M^T\right)^{-1} \\ B_{ki} = N^{-1}\left(\widehat{B}_i - SB_iD_{ki}\right) \\ A_{ki} = N^{-1}\left[\widehat{A}_i - S\left(A_i + B_iD_{ki}C\right)R\right]\left(M^T\right)^{-1} \\ \quad -B_{ki}CR\left(M^T\right)^{-1} - N^{-1}SB_iC_{ki} \end{cases} \tag{26}$$

Therefore, the local output feedback controller $U_i = K_iY$ is obtained.

Multiple output feedback control laws are obtained for different local linear system, and the following global output feedback control law is obtained by fuzzy synthesis of multiple fuzzy control laws.

$$U = \sum_{i=1}^{8} \overline{\mu}_i U_i = \sum_{i=1}^{8} \overline{\mu}_i (K_iY) \tag{27}$$

V. TORQUE DISTRIBUTION

The control signal outputted by the multi-objective controller is $U = [u_1, u_2, u_3]^T$, where u_1 is the torque difference between the left-front wheel and the right-front wheel, u_2 is the additional yaw moment, and u_3 is the driving torque. In this section, the control outputs u_1, u_2 and, u_3 are optimally distributed by calculating the constraint conditions and the optimization objective function to obtain the target torque of each in-wheel motor. The detailed torque distribution process can be found in the past study [41].

Minimizing tire load utilization is taken as the optimization objective function of the torque distribution.

$$J = min \sum_{i=1}^{4} \frac{T_{xi}^2}{(\mu F_{zi} r)^2} \tag{28}$$

The constraint conditions are as follows.

$$\begin{cases} T_{fl} + T_{fr} + T_{rl} + T_{rr} = u_3 \\ T_{fl} - T_{fr} = u_1 \\ \frac{l_s(T_{fl} - T_{fr} + T_{rl} - T_{rr})}{2r} = u_2 \\ T_i \le min\left(\mu F_{zi} r, T_{max}\right) \end{cases} \tag{29}$$

The equations with two variables T_{fl} and T_{fr} are obtained by using the eliminating method to process the constraint conditions shown in (29). The equations are substituted into (28), and the partial derivatives of T_{fl} and T_{fr} are calculated respectively to obtain the following optimal torque of each in-wheel motor.

$$\begin{cases} T_{fl} = \frac{\frac{u_3}{2} - \frac{ru_2}{l_s}}{(\mu F_{z4} r)^2} \Big/ \left[\frac{1}{(\mu F_{z2} r)^2} + \frac{1}{(\mu F_{z4} r)^2}\right] + u_1 \\ T_{fr} = \frac{\frac{u_3}{2} - \frac{ru_2}{l_s}}{(\mu F_{z4} r)^2} \Big/ \left[\frac{1}{(\mu F_{z2} r)^2} + \frac{1}{(\mu F_{z4} r)^2}\right] \\ T_{rl} = \frac{ru_2}{l_s} + \frac{u_3}{2} - T_{fl} \\ T_{rr} = \frac{u_3}{2} - \frac{ru_2}{l_s} - T_{fr} \end{cases} \tag{30}$$

VI. HARDWARE IN THE LOOP TEST RESULTS

The verification for the effectiveness of the designed trajectory tracking multi-objective controller is carried out by HIL test. The driving simulator is adopted as the core device where the PXI real-time system is utilized for the hardware in HIL test. Vehicle model and desired trajectory are established in the CarMaker software. The T-S fuzzy model, in-wheel motor model, the multi-objective control algorithm and the torque

$$\begin{cases} \begin{bmatrix} A_iR + RA_i^T + B_i\widehat{C}_i + \left(B_i\widehat{C}_i\right)^T & \widehat{A}_i^T + A_i + B_i\widehat{D}_iC & B_{1i} + B_i\widehat{D}_iD \\ * & SA_i + A_i^TS + \widehat{B}_iC + \left(\widehat{B}_iC\right)^T & SB_{1i} + \widehat{B}_iD \\ * & * & -I_1 \end{bmatrix} < 0 \\ \begin{bmatrix} R & I & R^TC_{11}^T \\ * & S & C_{11}^T \\ * & * & \lambda_1 I_2 \end{bmatrix} > 0 \\ \begin{bmatrix} A_iR + RA_i^T + B_i\widehat{C}_i + \left(B_i\widehat{C}_i\right)^T & \widehat{A}_i^T + A_i + B_i\widehat{D}_iC & B_{1i} + B_i\widehat{D}_iD & R^TC_{12}^T \\ * & SA_i + A_i^TS + \widehat{B}_iC + \left(\widehat{B}_iC\right)^T & SB_{1i} + \widehat{B}_iD & C_{12}^T \\ * & * & -\lambda_2 I_1 & D_{12}^T \\ * & * & * & \lambda_2 I_3 \end{bmatrix} < 0 \\ \begin{bmatrix} A_iR + RA_i^T + B_i\widehat{C}_i + \left(B_i\widehat{C}_i\right)^T & \widehat{A}_i^T + A_i + B_i\widehat{D}_iC \\ * & SA_i + A_i^TS + \widehat{B}_iC + \left(\widehat{B}_iC\right)^T \end{bmatrix} < 0 \\ \begin{bmatrix} R & I \\ * & S \end{bmatrix} > 0 \end{cases} \tag{24}$$

distribution algorithm are input in PXI real-time system. The comparison between the multi-objective controller and the single-objective controller is carried out in the test, where the multi-objective controller is the method designed in this paper and the single-objective controller is only considering the control objective of trajectory tracking accuracy. Results of the single-objective control are obtained by using the generalized H_2 norm to constrain the trajectory tracking error. Vehicle model parameters are shown in Table 1.

TABLE 1. Vehicle model parameters.

Symbol	Meaning	Value
m	Vehicle mass	650 kg
I_z	Moment of inertia around the z-axle	490 kg $\cdot$ m^2
l_f	Distance from the mass center to the front axles	0.74 m
l_r	Distance from the mass center to the rear axles	0.64 m
l_s	Wheel base	1.17 m
C_f	Cornering stiffness of front wheel	-45680 N/rad
C_r	Cornering stiffness of rear wheel	-45680 N/rad
r	Effective rolling radius of wheel	0.292 m

HIL test platform constitution framework is given in Fig. 4, which mainly includes the driving simulator, PXI real-time system, host computer and hardware platform. The hardware platform provides the power supply and function modules used in the platform. Multi-objective comprehensive controller designed in MATLAB/ Simulink are compiled and downloaded by the host computer to PXI-8840 real-time processor in PXI real-time system to generate control signal. The PXI real-time system sends the control signal to the actuators in the driving simulator through the PXI-8510 board. Concurrently, the control signal from the PXI-8840 in PXI real-time system is sent to the host computer installed with the dynamic software CarMaker for controlling the vehicle model driving on the virtual road.

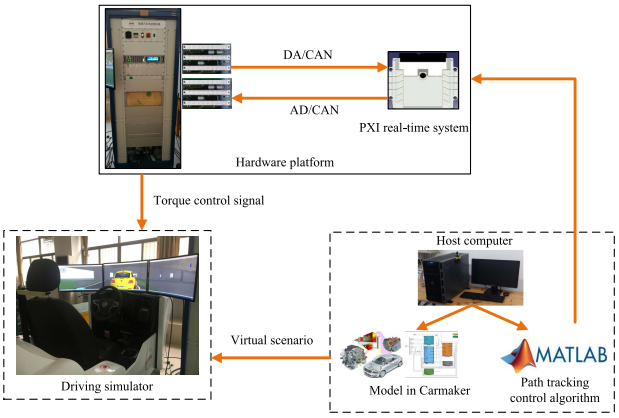

FIGURE 4. Framework of HIL test platform.

A. HIL TEST FOR J-TURN WITH ACCELERATING

A J-turn test path is constructed to evaluate the performance of the proposed multi-objective trajectory tracking controller. In the test process, 4MIDEV is accelerated from 30km/h, and the road adhesion coefficient is 0.8. The design parameters of the controller are set as $\lambda_1 = 1, \lambda_2 = 1.3$, the weighting coefficients of the controller are shown in Table 2, and the test results are shown in Fig. 5.

TABLE 2. Weighting coefficients of the controller.

k_1	k_2	k_3	k_4	k_5	k_6	k_7	k_8	k_9
100	0.1	4	40	1	10	30	3	8

The comparison of test results is shown in Table 3. The control method I represents the single-objective controller on the high adhesion road ($\mu = 0.8$), the control method II represents the single-objective controller on the low adhesion road ($\mu = 0.3$), the control method III represents the multi-objective controller on the high adhesion road ($\mu = 0.8$), and the control method IV represents the multi-objective controller on the low adhesion road ($\mu = 0.3$).

It can be seen from Fig. 5(a) that no matter on the high adhesion road or on the low adhesion road, the actual longitudinal speed of 4MIDEV controlled by the multi-objective controller can better track the expected longitudinal speed without fluctuation, while the longitudinal speed fluctuates significantly at 5.5s with the single object control. The reason for that the longitudinal speed curves fluctuation under the single-objective control is the trajectory curvature changes greatly at 5.5s, and the differential steering system comes into operation at that time. The test results also show that the differential steering has an impact on the vehicle longitudinal speed. The better longitudinal speed tracking effect under the multi-objective control indirectly indicates that the designed H_∞ performance index has certain robustness to the disturbances to the changes of the trajectory curvature and the road adhesion coefficient. It can be seen from Fig. 5(b) that the maximum value of the trajectory curvature is 0.014.

The comparison of methods III and I in Table 3 shows that although the multi-objective control on the high adhesion road has a slight decrease in the aspect of trajectory tracking accuracy compared with the single-objective control on the high adhesion road condition, it has a significant improvement in vehicle lateral stability. The reason why the trajectory tracking accuracy of the single-objective control is better than that of the multi-objective control, is that for single-objective control, only one target of trajectory tracking accuracy is paid attention to, and it does not consider vehicle lateral stability and longitudinal speed tracking performance. Thus, the trajectory tracking accuracy is higher. However, the multi-objective control is a compromise solution after comprehensively considering the trajectory tracking accuracy, the vehicle lateral dynamics performance and longitudinal speed tracking ability.

According to the comparison of control methods IV and II, the trajectory tracking accuracy with the multi-objective control and single-objective control are basically consistent on low adhesion road, while 4MIDEV with the multi-objective

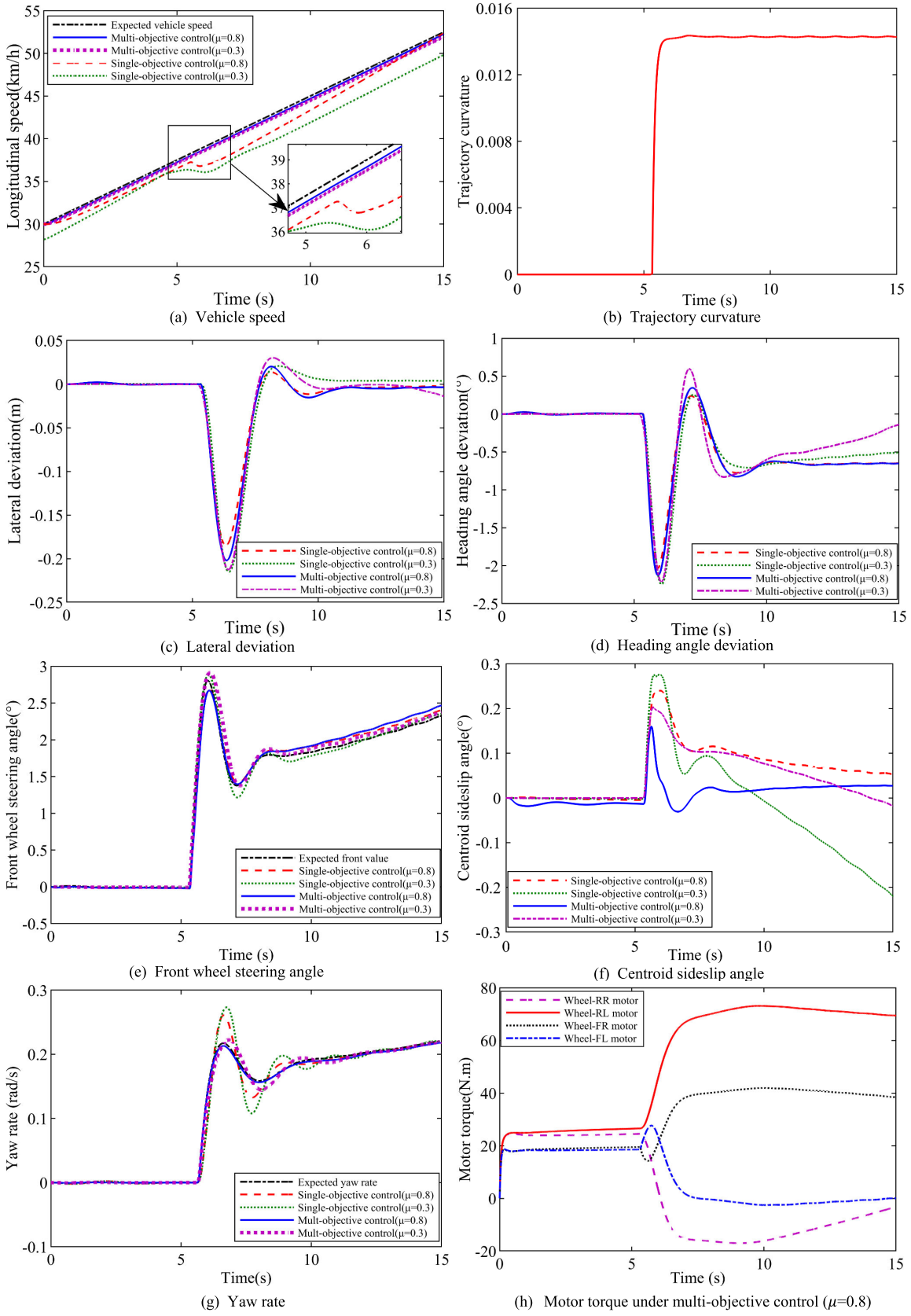

FIGURE 5. Results of J-Turn with accelerating.

TABLE 3. Result comparison of J-Turn with accelerating.

Control method	Peak value of lateral deviation e/m	Peak value of heading angle deviation ψ/deg	Peak value of centroid sideslip angle β/deg	Peak value of yaw rate tracking error $\dot{e}_3$/(rad/s)
I	0.186	2.036	0.238	0.044
II	0.215	2.248	0.276	0.072
III	0.201	2.126	0.164	0.018
IV	0.212	2.214	0.198	0.025
II compared to I	Increased 15.6%	Increased 10.4%	Increased 16.0%	Increased 63.6%
III compared to I	Increased 8.1%	Increased 4.4%	Decreased 31.1%	Decreased 59.1%
III compared to II	Decreased 6.5%	Decreased 5.4%	Decreased 40.6%	Decreased 75.0%
IV compared to I	Increased 14.0%	Increased 8.7%	Decreased 16.8%	Decreased 43.2%
IV compared to II	Decreased 1.4%	Decreased 1.5%	Decreased 28.3%	Decreased 65.3%
IV compared to III	Increased 5.5%	Increased 4.1%	Increased 20.7%	Increased 38.9%

control has better lateral stability. We can be concluded that compared with the single-objective control, the multi-objective controller has great advantage in improving the 4MIDEV lateral stability, and the trajectory tracking accuracy of the single-objective control is better than that of the multi-objective control under the condition of high adhesion road, while the trajectory tracking accuracy of the single target control cannot be significantly improved under the condition of low adhesion road. The comparison of control methods IV and I also show that the multi-objective control plays an important role in improving 4MIDEV lateral stability. According to the comparison of control methods II and I and the comparison of control methods IV and III, it can be concluded that when the road adhesion coefficient is reduced, the performance of single objective control, such as trajectory tracking accuracy and vehicle lateral stability, will be greatly degraded, while the performance of the multi-objective controller will be slightly degraded. The multi-objective controller has good robustness to the changes of trajectory curvature and the road adhesion coefficient. The curves change in the Fig. 5(c), (d), (f), and (g) can also verify the above conclusion.

According to Fig. 5(e), the front-wheel steering angle curves with both the multi-objective control and single-objective control are basically coincide with the curves of the expected values on high or low adhesion road, the two controllers can track the expected front-wheel steering angle well. It can be seen from Fig. 5(h) that the torque of the right front wheel motor is bigger than that of the left front wheel motor at 5.5s, and with the action of front-wheel torque difference, the vehicle turns left. Correspondingly, the positive front wheel steering angle in Fig. 5(e) indicates the left turning of the vehicle. The torque difference between the left front wheel motor and the right front wheel motor introduces an additional counterclockwise yaw moment at 5.5s. To counteract this yaw moment, the torque of the left rear wheel motor is greater than that of the right rear wheel motor, a clockwise yaw moment is generated onto 4MIDEV to eliminate the impact of differential steering on vehicle lateral stability performance. It is worth noting that the motor torque variation under the multi-objective control on the low adhesion road is similar to that on the high adhesion road. In order to avoid repetition, only the motor torque variation under multi-objective control on the high adhesion road is given in Fig. 5(h) and similar observations can be found in [42].

B. HIL TEST FOR DOUBLE LANE CHANGE WITH ACCELERATING

In order to test 4MIDEV trajectory tracking performance during the acceleration overtaking process, HIL test is carried out under double lane change (DLC) trajectory tracking condition. The road adhesion coefficient is set as 0.8 and 0.3 respectively, 4MIDEV longitudinal speed accelerated from 30km/h, and the controller design parameters are consistent with that under the J-Turn trajectory tracking condition. The weighting coefficients of the controller are shown in Table 2, and the test results are shown in Fig. 6.

Longitudinal speed tracking performance is shown in Fig. 6(a). It can be seen that the multi-objective controller achieves good longitudinal velocity tracking effect on the road with two kinds of adhesion coefficients, while the deviation between the longitudinal speed of 4MIDEV controlled by the single-objective controller and the target speed is large. Single-objective control cannot eliminate the influence of differential steering on longitudinal speed, and the longitudinal speed fluctuation is obvious at 5.5s∼8.5s.

According to Fig. 6(c), the lateral deviation performance of single-objective control is poor on the low adhesion road, the maximum lateral deviation is big up to 0.28m, so the limitation of single-objective control is displayed. It can be found out from Fig. 6(d) that the performance of the two controllers is similar in the aspect of heading angle control. Similar to the test of J-turn with accelerating, the multi-objective controller plays an important role in improving 4MIDEV lateral stability according to Fig. 6(f) and (g). Besides, we found out that the too large centroid sideslip angle controlled by single-objective controller may cause dangerous situation on the low adhesion road.

As shown in Fig. 6(e), on the high adhesion road, the front-wheel steering angle curves under the multi-objective control is basically coincide with the curve of the expected values, so that the multi-objective controller can track the

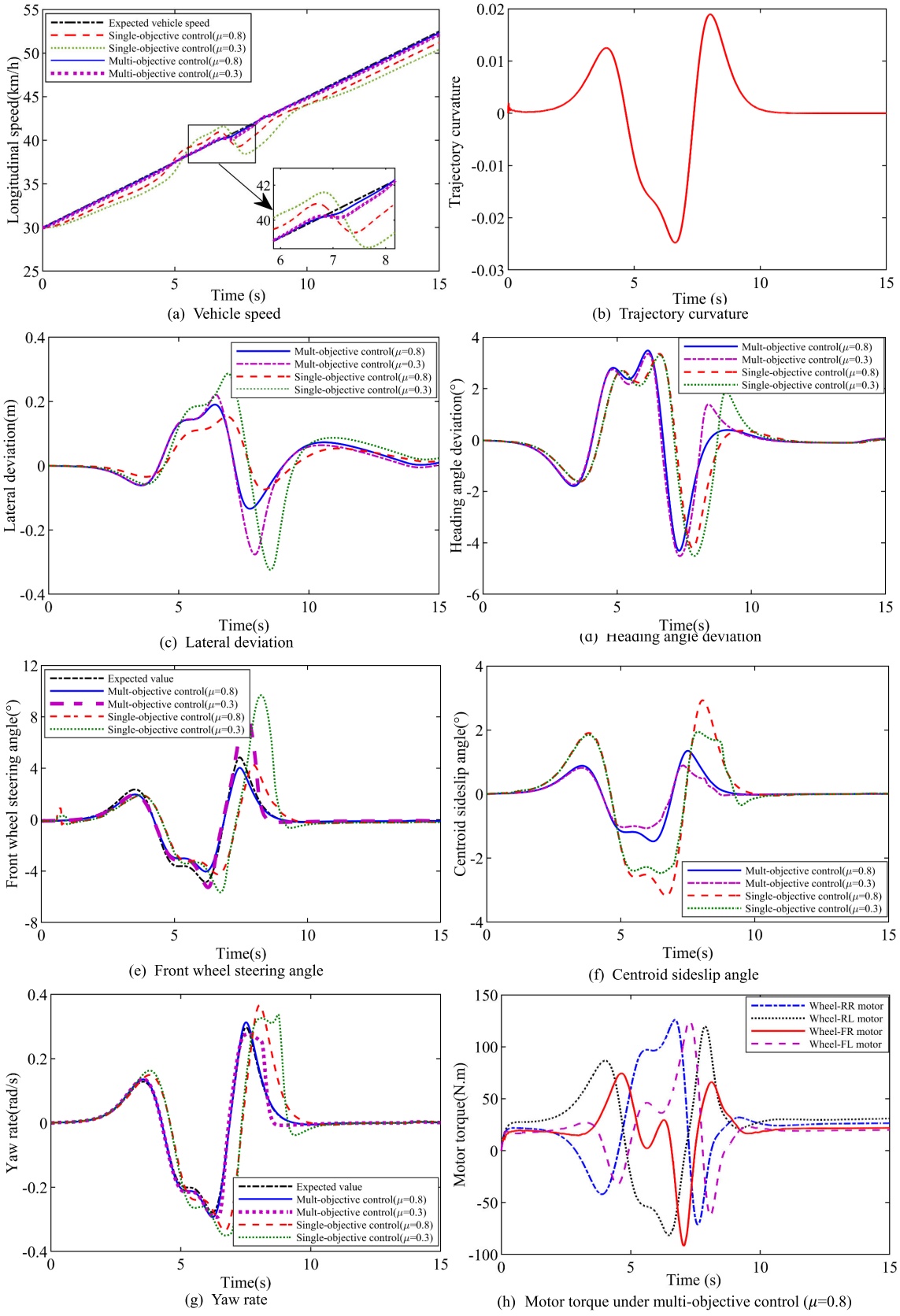

FIGURE 6. Results of DLC with accelerating.

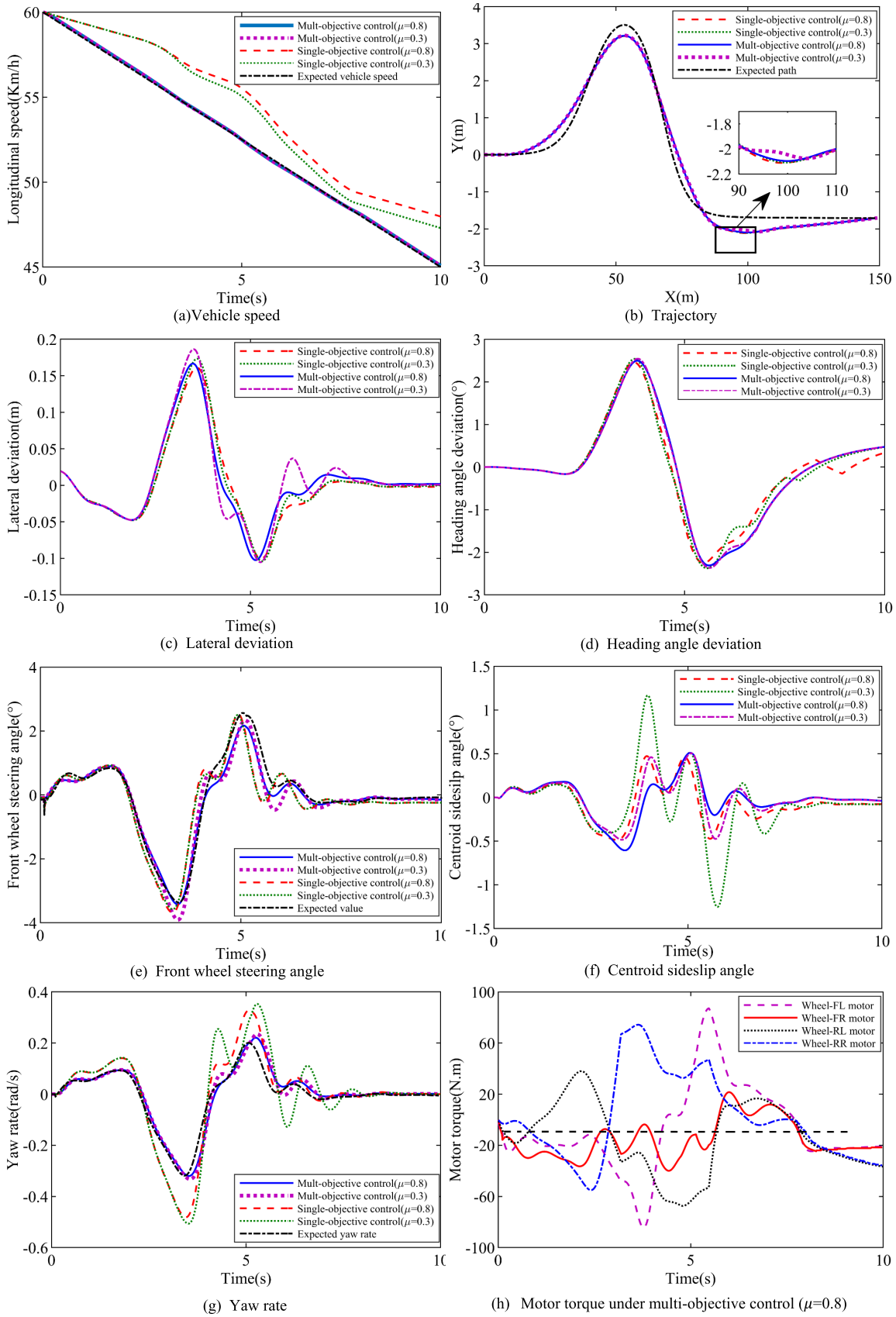

FIGURE 7. Results of DLC with decelerating.

expected steering angle well; and on the low adhesion road, the multi-objective control generates a large front wheel angle to maintain lateral stability. It can be seen from Fig. 6(h) that the front-wheel torque difference is large at 3.9s, 6.6s and 8.0s, and the trajectory curvatures shown in Fig. 6(b) are also relatively large at these times, which also corresponds to the larger expected front-wheel steering angle in the Fig. 6(e).

C. HIL TEST FOR DOUBLE LANE CHANGE WITH DECELERATING

The test results of the previous two subsections verify the performance of the multi-objective controller under the acceleration conditions. Now, 4MIDEV is set to travel in the path shown in Fig. 7(b). In this maneuver, the vehicle is required to complete DLC action within 15s and decelerate from 60 km/h to 45 km/h. The test is carried out on high adhesion coefficient pavement and low adhesion coefficient pavement respectively. According to Fig. 7(a)∼(g), the multi-objective controller designed in this paper can achieve a high trajectory tracking accuracy. Although the trajectory tracking error is increased slightly compared with the single-objective control, the increased degree of the trajectory tracking error is small. The vehicle lateral stability and longitudinal speed tracking performance are improved significantly with the multi-objective control. As shown in Fig. 7(h), when the multi-objective controller is adopted, the negative torque is generated by four in-wheel motors to make the vehicle brake and keep the vehicle speed near the expected speed, where the effect of vehicle speed control is shown in Fig. 7(a). According to Fig. 7(b) and (h), when the vehicle heading changes at 2.3s, 3.8s, and 5.5s, vehicle body will produce large yaw motion amplitudes. The multi-objective control applies the large positive driving torque to the rear-left wheel, rear-right wheel and front-left wheel to generate enough yaw moments respectively, so as to stabilize the body attitude and minimize the centroid sideslip angle shown in Fig. 7(f) and make the actual yaw rate shown in Fig. 7(g) match the expected yaw rate. Therefore, the designed multi-objective controller can effectively improve the comprehensive performance of 4MIDEV, while taking into account the trajectory tracking accuracy and the longitudinal and lateral dynamics characteristics.

VII. CONCLUSION

The trajectory tracking multi-objective controller for 4MIDEV with differential steering is studied in this paper. Firstly, according to the differential steering dynamics characteristics, the dynamics model of 4MIDEV with differential steering is established. The system state equation is obtained by combining the dynamics model of 4MIDEV with differential steering, the in-wheel motor model and the trajectory tracking model. Then, considering there are nonlinear time-varying parameters such as the vehicle speed and the front wheel steering angle in the coefficient matrixes of the system state equation, which brings difficulty to the controller design. Therefore, the T-S fuzzy method is utilized to process the nonlinear time-varying parameters, and the system T-S fuzzy state equation is obtained. Finally, the kinematics control output, dynamics control output and the measurement output of the system are selected, and the system's T-S fuzzy model is finally obtained. The influence of differential steering on the vehicle longitudinal and lateral dynamics characteristics is fully considered, and the trajectory tracking control of 4MIDEV is taken as a multi-objective control problem in this paper. The high trajectory tracking accuracy, good vehicle lateral stability and longitudinal speed tracking performance are taken as the control objectives of the trajectory tracking control.

Considering that the trajectory tracking control of 4MIDEV is not only a multi-objective control problem, but also a vehicle kinematics and dynamics integration control problem. The trajectory tracking geometric error is attributed to the vehicle kinematics category, and the vehicle longitudinal and lateral dynamics characteristics are attributed to the vehicle dynamics category. The generalized H_2 norm and the H_∞ norm are selected to constrain the kinematics and dynamics performance indexes of trajectory tracking. The parallel distributed compensation method is adopted to design the multi-objective output feedback controller for the system T-S fuzzy model. Finally, HIL test is adopted to verify the effectiveness of the designed trajectory tracking multi-objective control system. The considerable results show that the multi-objective control method can effectively improve the comprehensive performance of the control system.

REFERENCES

[1] C. Chatzikomis, M. Zanchetta, P. Gruber, A. Sorniotti, B. Modic, T. Motaln, L. Blagotinsek, and G. Gotovac, "An energy-efficient torque-vectoring algorithm for electric vehicles with multiple motors," *Mech. Syst. Signal Process.*, vol. 128, pp. 655–673, Aug. 2019, doi: 10.1016/j.ymssp.2019.03.012.

[2] Z. Li, L. Zheng, W. Gao, and Z. Zhan, "Electromechanical coupling mechanism and control strategy for in-wheel-motor-driven electric vehicles," *IEEE Trans. Ind. Electron.*, vol. 66, no. 6, pp. 4524–4533, Jun. 2019, doi: 10.1109/TIE.2018.2863204.

[3] M. Kuslits and D. Bestle, "Modelling and control of a new differential steering concept," *Vehicle Syst. Dyn.*, vol. 57, no. 4, pp. 520–542, Apr. 2019, doi: 10.1080/00423114.2018.1473616.

[4] C. Hu, R. Wang, F. Yan, Y. Huang, H. Wang, and C. Wei, "Differential steering based yaw stabilization using ISMC for independently actuated electric vehicles," *IEEE Trans. Intell. Transp. Syst.*, vol. 19, no. 2, pp. 627–638, Feb. 2018, doi: 10.1109/TITS.2017.2750063.

[5] Z. Tang, X. Xu, F. Wang, X. Jiang, and H. Jiang, "Coordinated control for path following of two-wheel independently actuated autonomous ground vehicle," *IET Intell. Transp. Syst.*, vol. 13, no. 4, pp. 628–635, Apr. 2019, doi: 10.1049/iet-its.2018.5065.

[6] X. Xu, L. Shanfeng, C. Long, C. Yingfeng, and L. Yong, "Trajectory tracking of distributed-drive self-driving vehicle based on coordination between autonomous steering and differential steering," *Automot. Eng.*, vol. 40, no. 4, pp. 475–481, 2018.

[7] J. Tian, J. Tong, and S. Luo, "Differential steering control of four-wheel independent-drive electric vehicles," *Energies*, vol. 11, no. 11, pp. 2892–2909, 2018, doi: 10.3390/en11112892.

[8] J. Wang, Z. Luo, Y. Wang, B. Yang, and F. Assadian, "Coordination control of differential drive assist steering and vehicle stability control for four-wheel-independent-drive EV," *IEEE Trans. Veh. Technol.*, vol. 67, no. 12, pp. 11453–11467, Dec. 2018, doi: 10.1109/TVT.2018.2872857.

[9] R. Wang, H. Jing, C. Hu, M. Chadli, and F. Yan, "Robust H∞ output-feedback yaw control for in-wheel motor driven electric vehicles with differential steering," *Neurocomputing*, vol. 173, pp. 676–684, Jan. 2016, doi: 10.1016/j.neucom.2015.08.015.

[10] C. Hu, R. Wang, F. Yan, and H. R. Karimi, "Robust composite nonlinear feedback path-following control for independently actuated autonomous vehicles with differential steering," *IEEE Trans. Transport. Electrific.*, vol. 2, no. 3, pp. 312–321, Sep. 2016, doi: 10.1109/TTE.2016.2538183.

[11] W. Zhao and H. Zhang, "Coupling control strategy of force and displacement for electric differential power steering system of electric vehicle with motorized wheels," *IEEE Trans. Veh. Technol.*, vol. 67, no. 9, pp. 8118–8128, Sep. 2018, doi: 10.1109/TVT.2018.2850154.

[12] D. Hernandez-Alcantara, L. Amezquita-Brooks, R. Morales-Menendez, O. Sename, and L. Dugard, "The cross-coupling of lateral-longitudinal vehicle dynamics: Towards decentralized fault-tolerant control schemes," *Mechatronics*, vol. 50, pp. 377–393, Apr. 2018, doi: 10.1016/j.mechatronics.2017.07.001.

[13] C. E. Beal and C. Boyd, "Coupled lateral-longitudinal vehicle dynamics and control design with three-dimensional state portraits," *Vehicle Syst. Dyn.*, vol. 57, no. 2, pp. 286–313, Feb. 2019, doi: 10.1080/00423114.2018.1467019.

[14] R. Zhang, Y. Ma, Z. Li, R. Malekian, and M. A. Sotelo, "Energy dissipation based longitudinal and lateral coupling control for intelligent vehicles," *IEEE Intell. Transp. Syst. Mag.*, vol. 10, no. 2, pp. 121–133, Summer 2018, doi: 10.1109/MITS.2018.2806623.

[15] X. Jin, Z. Yu, G. Yin, and J. Wang, "Improving vehicle handling stability based on combined AFS and DYC system via robust Takagi-Sugeno fuzzy control," *IEEE Trans. Intell. Transp. Syst.*, vol. 19, no. 8, pp. 2696–2707, Aug. 2018, doi: 10.1109/TITS.2017.2754140.

[16] X. Jin, G. Yin, and J. Wang, "Robust fuzzy control for vehicle lateral dynamic stability via Takagi-Sugeno fuzzy approach," in *Proc. Amer. Control Conf. (ACC)*, May 2017, pp. 5574–5579, doi: 10.23919/ACC.2017.7963822.

[17] A. Cherifi, K. Guelton, and L. Arcese, "Uncertain T-S model-based robust controller design with $\mathcal{D}$-stability constraints—A simulation study of quadrotor attitude stabilization," *Eng. Appl. Artif. Intell.*, vol. 67, pp. 419–429, Jan. 2018, doi: 10.1016/j.engappai.2017.08.021.

[18] R.-E. Precup, M.-C. Sabau, and E. M. Petriu, "Nature-inspired optimal tuning of input membership functions of Takagi-Sugeno-Kang fuzzy models for anti-lock braking systems," *Appl. Soft Comput.*, vol. 27, pp. 575–589, Feb. 2015, doi: 10.1016/j.asoc.2014.07.004.

[19] X. Ji, Y. Liu, X. He, K. Yang, X. Na, C. Lv, and Y. Liu, "Interactive control paradigm-based robust lateral stability controller design for autonomous automobile path tracking with uncertain disturbance: A dynamic game approach," *IEEE Trans. Veh. Technol.*, vol. 67, no. 8, pp. 6906–6920, Aug. 2018, doi: 10.1109/TVT.2018.2834381.

[20] S. Yuan, P. Zhao, Q. Zhang, and X. Hu, "Research on model predictive control-based trajectory tracking for unmanned vehicles," in *Proc. 4th Int. Conf. Control Robot. Eng. (ICCRE)*, Apr. 2019, pp. 79–86, doi: 10.1109/ICCRE.2019.8724158.

[21] C. Bian, G. Yin, N. Zhang, and L. Xu, "Takagi-sugeno fuzzy model predictive controller design for combining lane keeping and speed tracking of four wheels steering and four wheels drive electric vehicle," in *Proc. 29th Chin. Control Decis. Conf. (CCDC)*, May 2017, pp. 4067–4072, doi: 10.1109/CCDC.2017.7979212.

[22] B. Li, H. Du, and W. Li, "A potential field approach-based trajectory control for autonomous electric vehicles with in-wheel motors," *IEEE Trans. Intell. Transp. Syst.*, vol. 18, no. 8, pp. 2044–2055, Aug. 2017, doi: 10.1109/TITS.2016.2632710.

[23] L. Guo, P. Ge, M. Yue, and J. Li, "Trajectory tracking algorithm in a hierarchical strategy for electric vehicle driven by four independent in-wheel motors," *J. Chin. Inst. Eng.*, vol. 43, no. 8, pp. 807–818, Nov. 2020, doi: 10.1080/02533839.2020.1819432.

[24] P. Hang, F. Luo, S. Fang, and X. Chen, "Path tracking control of a four-wheel-independent-steering electric vehicle based on model predictive control," in *Proc. 36th Chin. Control Conf. (CCC)*, 2017, pp. 9360–9366, doi: 10.23919/ChiCC.2017.8028849.

[25] H. Zheng and S. Yang, "A trajectory tracking control strategy of 4WIS/4WID electric vehicle with adaptation of driving conditions," *Appl. Sci.*, vol. 9, no. 1, p. 168, Jan. 2019, doi: 10.3390/app9010168.

[26] Z. Wang, D. Tan, G. Ge, and S. Liu, "Optimal trajectory planning and control for automatic lane change of in wheel motor driving vehicles on snow and ice roads," *Autom. Control Comput. Sci.*, vol. 54, no. 5, pp. 432–445, Sep. 2020, doi: 10.3103/S0146411620050090.

[27] F. Lin, Y. Zhang, Y. Zhao, G. Yin, H. Zhang, and K. Wang, "Trajectory tracking of autonomous vehicle with the fusion of DYC and longitudinal–lateral control," *Chin. J. Mech. Eng.*, vol. 32, no. 1, p. 16, Dec. 2019, doi: 10.1186/s10033-019-0327-9.

[28] D. V. Balandin and M. M. Kogan, "LMI based multi-objective control under multiple integral and output constraints," *Int. J. Control*, vol. 83, no. 2, pp. 227–232, Feb. 2010, doi: 10.1080/00207170903134130.

[29] C. Han and D. Zhao, "Multi-objective static output feedback control for vehicle active suspension," in *Proc. IEEE Int. Conf. Mechatronics Autom.*, Aug. 2014, pp. 1526–1532, doi: 10.1109/ICMA.2014.6885926.

[30] X. Jin, J. Wang, S. Sun, S. Li, J. Yang, and Z. Yan, "Design of constrained robust controller for active suspension of in-wheel-drive electric vehicles," *Mathematics*, vol. 9, no. 3, p. 249, Jan. 2021, doi: 10.3390/math9030249.

[31] Y. Hu, Y. Yuan, H. Min, and F. Sun, "Multi-objective robust control based on fuzzy singularly perturbed models for hypersonic vehicles," *Sci. China Inf. Sci.*, vol. 54, no. 3, pp. 563–576, Mar. 2011.

[32] H. Zhou, F. Jia, H. Jing, Z. Liu, and L. Guvenc, "Coordinated longitudinal and lateral motion control for four wheel independent motor-drive electric vehicle," *IEEE Trans. Veh. Technol.*, vol. 67, no. 5, pp. 3782–3790, May 2018, doi: 10.1109/TVT.2018.2816936.

[33] W. Chen, W. Xiao, D. Tan, S. Lin, X. Sun, and Y. Xie, "Study on the grey predictive extension control of yaw stability of electric vehicle based on the minimum energy consumption," *J. Mech. Eng.*, vol. 55, no. 2, pp. 156–167, 2019.

[34] R. Wang, G. Yin, and X. Jin, "Robust adaptive sliding mode control for nonlinear four-wheel steering autonomous vehicles path tracking systems," in *Proc. IEEE 8th Int. Power Electron. Motion Control Conf. (IPEMC-ECCE Asia)*, May 2016, pp. 2999–3006, doi: 10.1109/IPEMC.2016.7512774.

[35] K. T. Leung, J. F. Whidborne, D. Purdy, and P. Barber, "Road vehicle state estimation using low-cost GPS/INS," *Mech. Syst. Signal Process.*, vol. 25, no. 6, pp. 1988–2004, Aug. 2011, doi: 10.1016/j.ymssp.2010.08.003.

[36] A.-T. Nguyen, C. Sentouh, and J.-C. Popieul, "Sensor reduction for driver-automation shared steering control via an adaptive authority allocation strategy," *IEEE/ASME Trans. Mechatronics*, vol. 23, no. 1, pp. 5–16, Feb. 2018, doi: 10.1109/TMECH.2017.2698216.

[37] Z. Zhang, H. Liang, H. Ma, and Y. Pan, "Reliable fuzzy control for uncertain vehicle suspension systems with random incomplete transmission signals and sensor failure," *Mech. Syst. Signal Process.*, vol. 130, pp. 776–789, Sep. 2019, doi: 10.1016/j.ymssp.2019.05.032.

[38] R. Wang, C. Hu, F. Yan, and M. Chadli, "Composite nonlinear feedback control for path following of four-wheel independently actuated autonomous ground vehicles," *IEEE Trans. Intell. Transp. Syst.*, vol. 17, no. 7, pp. 2063–2074, Jul. 2016, doi: 10.1109/TITS.2015.2498172.

[39] Y. Ma, J. Chen, X. Zhu, and Y. Xu, "Lateral stability integrated with energy efficiency control for electric vehicles," *Mech. Syst. Signal Process.*, vol. 127, pp. 1–15, Jul. 2019, doi: 10.1016/j.ymssp.2019.02.057.

[40] J. Ni, W. Wang, J. Hu, and C. Xiang, "Relaxed static stability for four-wheel independently actuated ground vehicle," *Mech. Syst. Signal Process.*, vol. 127, pp. 35–49, Jul. 2019, doi: 10.1016/j.ymssp.2019.02.059.

[41] L. Guo, P. Ge, and D. Sun, "Torque distribution algorithm for stability control of electric vehicle driven by four in-wheel motors under emergency conditions," *IEEE Access*, vol. 7, pp. 104737–104748, 2019, doi: 10.1109/ACCESS.2019.2931505.

[42] J. Huang, Y. Liu, M. Liu, M. Cao, and Q. Yan, "Multi-objective optimization control of distributed electric drive vehicles based on optimal torque distribution," *IEEE Access*, vol. 7, pp. 16377–16394, 2019, doi: 10.1109/ACCESS.2019.2894259.

HONGBO WANG received the B.Tech., M.S., and Ph.D. degrees from the Hefei University of Technology, Hefei, China, in 2003, 2006, and 2014, respectively. He is currently an Associate Professor with the School of Automotive and Transportation Engineering, Hefei University of Technology. He has authored more than 50 articles. His current research interests include robust control, structured control, and control theory applied to automotive systems.

CHENGLEI HU received the B.Tech. degree from Nanjing Agricultural University, Nanjing, China, in 2018. He is currently pursuing the M.S. degree with the Hefei University of Technology, Hefei, China. His research interest includes vehicle dynamics and control, particularly the design of driver assistance systems.

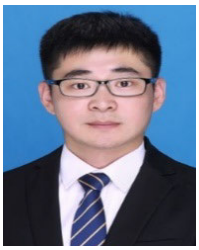

WEI CUI received the B.Tech. degree from Qingdao University, Qingdao, in 2017, and the M.S. degree from the Hefei University of Technology, Hefei, China, in 2020. He is currently pursuing the Ph.D. degree with Shandong University, China. His research interests include vehicle dynamics and control, and energy management optimization.

HAIPING DU (Senior Member, IEEE) received the Ph.D. degree in mechanical design and theory from Shanghai Jiao Tong University, Shanghai, China, in 2002.

He was a Postdoctoral Research Associate with The University of Hong Kong, from 2002 to 2003, and Imperial College London, from 2004 to 2005. He was a Research Fellow with the University of Technology Sydney, from 2005 to 2009. He is currently a Professor with the School of Electrical, Computer, and Telecommunications Engineering, University of Wollongong, Wollongong, NSW, Australia. His research interests include vibration control, vehicle dynamics and control systems, robust control theory and engineering applications, electric vehicles, robotics and automation, and smart materials and structures. He was a recipient of the Australian Endeavour Research Fellowship, in 2012. He is also a Subject Editor for the *Journal of the Franklin Institute*, an Associate Editor for the IEEE TRANSACTIONS ON INDUSTRIAL ELECTRONICS and IEEE Control Systems Society Conference, an Editorial Board Member for some international journals, such as *Journal of Sound and Vibration*, *Journal of Systems and Control Engineering* (IMechE), and a Guest Editor of *IET Control Theory and Applications* and *Mechatronics*.